Epistasis experiments. ΔArm was expressed using a *hs-Gal4* driver line in combination with a *UAS-Δarm* transgene[6]. Embryos were heat-shocked two or three times at 37 °C for 30 min with a recovery time of 2 to 3 h at 25 °C between heat shocks. To perform this experiment in pan^{13} or ci^{Cell} mutant backgrounds *yw, hs-Gal4/+*, pan^{13} (or ci^{Cell})/*Dp(1;4)1021*[y^+] females were crossed to *yw, UAS-Δarm/+*, pan^{13} (or ci^{Cell})/*Dp(1;4)1021*[y^+] males, and the progeny were subjected to the same heat-shock regime. *y* mutant cuticles were identified by scoring denticles, beard or residual lateral denticles. In the case of pan^{13}, we never observed a *y* mutant larva that showed reversal of the lawn phenotype. For the embryo shown in Fig. 4e, the experiment was repeated with progeny of *UAS-Δarm/UAS-Δarm*, pan^{13}/+ females crossed to *hs-Gal4/hs-Gal4*, pan^{13}/+ males.

Received 22 January; accepted 6 February 1997.

1. Nusse, R. & Varmus, H. E. *Cell* **69,** 1073–1087 (1992).
2. Danielian, P. S. & McMahon, A. P. *Nature* **383,** 332–334 (1996).
3. Li, X. & Noll, M. *EMBO J.* **12,** 4499–4509 (1993).
4. Yu, X., Hoppler, S., Eresh, S. & Bienz, M. *Development* **122,** 849–858 (1996).
5. Brook, W. J. & Cohen, S. M. *Science* **273,** 1373–1377 (1996).
6. Zecca, M., Basler, K. & Struhl, G. *Cell* **87,** 833–844 (1996).
7. Huber, O. *et al. Mech. Dev.* **59,** 3–10 (1996).
8. Molenaar, M. *et al. Cell* **86,** 391–399 (1996).
9. Behrens, J. *et al. Nature* **382,** 638–642 (1996).
10. Peifer, M. & Wieschaus, E. *Cell* **63,** 1167–1176 (1990).
11. Siegfried, E. & Perrimon, N. *BioEssays* **16,** 395–404 (1994).
12. Locke, J. & Tartof, K. D. *Mol. Gen. Genet.* **243,** 234–243 (1994).
13. Struhl, G. & Basler, K. *Cell* **72,** 527–540 (1993).
14. Couso, J. P., Bishop, S. A. & Martinez Arias, A. *Development* **120,** 621–636 (1994).
15. Peifer, M., Rauskolb, C., Williams, M., Riggleman, B. & Wieschaus, E. *Development* **111,** 1029–1043 (1991).
16. Baker, N. E. *Development* **102,** 489–497 (1988).
17. Morata, G. & Lawrence, P. A. *Dev. Biol.* **56,** 227–240 (1977).
18. Ng, M., Diaz, B. F., Vincent, J. P., Wu, J. & Cohen, S. M. *Nature* **381,** 316–318 (1996).
19. Phillips, R. G. & Whittle, J. R. S. *Development* **118,** 427–438 (1993).
20. Rulifson, E. J. & Blair, S. S. *Development* **121,** 2813–2824 (1995).
21. Diaz Benjumea, F. & Cohen, S. M. *Development* **121,** 4215–4225 (1995).
22. Shirras, A. D. & Couso, J. P. *Dev. Biol.* **175,** 24–36 (1996).
23. Hochman, B. *Genetica* **35,** 109–126 (1964).
24. Alexandre, C., Jacinto, A. & Ingham, P. W. *Genes Dev.* **10,** 2003–2013 (1996).
25. Motzny, C. K. & Holmgren, R. *Mech. Dev.* **52,** 137–150 (1995).
26. Slusarski, D. C., Motzny, C. K. & Holmgren, R. *Genetics* **139,** 229–240 (1995).
27. Dominguez, M., Brunner, M., Hafen, E. & Basler, K. *Science* **272,** 1621–1625 (1996).
28. Forbes, A. J., Nakano, Y., Taylo, A. M. & Ingham, P. W. *Development* **119,** 115–124 (1993).
29. Bejsovec, A. & Martinez Arias, A. *Development* **113,** 471–485 (1991).
30. Noordermeer, J., Johnston, P., Rijsewijk, F., Nusse, R. & Lawrence, P. A. *Development* **116,** 711–719 (1992).
31. Basler, K., Christen, B. & Hafen, E. *Cell* **64,** 1069–1081 (1991).
32. Cadigan, K. M. & Nusse, R. *Development* **122,** 2801–2812 (1996).
33. Hochman, B. *Genetics* **67,** 235–252 (1971).
34. Travis, A., Amsterdam, A., Belanger, C. & Grosschedl, R. *Genes Dev.* **5,** 880–894 (1991).
35. Lin, R., Thompson, S. & Priess, J. R. *Cell* **83,** 599–609 (1995).

Acknowledgements. We thank M. Affolter, O. Huber and R. Kemler for discussions, O. Huber for his invaluable help with the binding assays, A. Bejsovec, R. Holmgren, J. Locke and the Bowling Green Stock Center for stocks, and E. Hafen, N. Méthot and G. Struhl for comments on the manuscript. This work was supported by the Swiss National Science Foundation and the Kanton of Zürich.

Correspondence and requests for materials should be addressed to K.B. (e-mail: basler@zool.unizh.ch). The GenBank accession number for *pan* is U88538.

Crystal structure of the anthrax toxin protective antigen

Carlo Petosa*, R. John Collier†, Kurt R. Klimpel‡, Stephen H. Leppla‡ & Robert C. Liddington*

* *Biochemistry Department, University of Leicester, Leicester LE1 7RH, UK*
† *Department of Microbiology & Molecular Genetics, 200 Longwood Avenue, Harvard Medical School, Boston, Massachusetts 02115, USA*
‡ *Laboratory of Microbial Ecology, Building 30, Room 309, National Institute of Dental Research, National Institutes of Health, Bethesda, Maryland 20982, USA*

Protective antigen (PA) is the central component of the three-part protein toxin secreted by *Bacillus anthracis*, the organism responsible for anthrax[1]. After proteolytic activation on the host cell surface, PA forms a membrane-inserting heptamer that translocates the toxic enzymes, oedema factor and lethal factor, into the cytosol[2–4]. PA, which has a relative molecular mass of 83,000 (M_r 83K), can also translocate heterologous proteins, and is being evaluated for use as a general protein delivery system[5,6]. Here we report the crystal structure of monomeric PA at 2.1 Å resolution and the water-soluble heptamer at 4.5 Å resolution. The monomer is organized mainly into antiparallel β-sheets and has four domains: an amino-terminal domain (domain 1) containing two calcium ions and the cleavage site for activating proteases; a heptamerization domain (domain 2) containing a large flexible loop implicated in membrane insertion; a small domain of unknown function (domain 3); and a carboxy-terminal receptor-binding domain (domain 4). Removal of a 20K amino-terminal fragment from domain 1 allows the assembly of the heptamer, a ring-shaped structure with a negatively charged lumen, and exposes a large hydrophobic surface for binding the toxic enzymes. We propose a model of pH-dependent membrane insertion involving the formation of a porin-like, membrane-spanning β-barrel.

Protective antigen, named for its use in vaccines, is a long, flat molecule of dimensions 100 × ~50 × 30 Å (Fig. 1b). Domain 1 (residues 1–258) comprises a β-sandwich with jelly-roll topology, several small helices, and a pair of adjacent calcium ions coordinated by residues in a variant of the EF-hand motif (Fig. 2a, b). Domain 2 (residues 259–487) has a β-barrel core with modified Greek-key topology and elaborate excursions, including a large flexible loop between strands $2\beta_2$ and $2\beta_3$ that is implicated in membrane insertion (Fig. 2c). Domain 3 (residues 488–595) has a four-stranded mixed β-sheet, two smaller sheets and four helices (Fig. 2d); it adopts the same fold as ferredoxins and resembles domain A of toxic-shock-syndrome toxin-1 (ref. 7). Domain 4 (residues 596–735) has an initial hairpin and helix, followed by a β-sandwich with an immunoglobulin-like fold (Fig. 2e). Domains 1, 2 and 3 are intimately associated, but domain 4 has limited contact with them.

Homologues of PA have been found in several spore-forming Gram-positive bacteria (for example, the iota-*b* toxin in *Clostridium perfringens*[8] and the vegetative insecticidal protein (VIP1) toxins in *Bacillus cereus* and *B. thuringiensis*[9]) and share the ability to translocate toxic enzymes into the host cytosol. High sequence similarity over the first 600 residues and strictly conserved calcium-binding motifs indicate that the homologues share the same folds for domains 1, 2 and 3 (Fig. 1c).

The steps in host-cell intoxication are illustrated in Fig. 1a. Studies with blocking antibodies[10], proteolytic fragments[11] and deletion mutants[12] implicate domain 4 in host-cell binding. Within the immunoglobulin-like fold, a 19-residue, highly accessible loop (between strands $4\beta_9$ and $4\beta_{10}$) is analogous to the antigen-binding CDR3 loop of antibodies and the receptor-binding loop of diphtheria toxin[13]. The loop is a good candidate for mediating the interaction between PA and the receptor, as short carboxy-terminal deletions that compromise the integrity of this loop eliminate cell binding (Fig. 2e).

Proteolytic activation by the cell-surface protease furin occurs in a surface loop within domain 1, releasing an N-terminal 20K fragment, PA_{20} (residues 1–167), which plays no further role in intoxication. PA_{20} forms an integral part of domain 1 (Fig. 2a), and dissociation requires the rupture of a β-sheet (between strands $1\beta_2$ and $1\beta_{13}$) and exposure of a large hydrophobic surface. This explains why PA can be 'nicked' *in vitro* at the furin site without dissociating into two fragments[14]. The remainder of domain 1, which we call domain 1′ (residues 168–258), forms the N terminus of the active 63K fragment, PA_{63}.

Loss of PA_{20} leads to heptamer formation by PA_{63} (ref. 4). The heptamer is water soluble at neutral or basic pH, and inserts into membranes at acidic pH, forming cation-selective channels in both artificial lipid bilayers[15] and cells[3]. The water-soluble heptamer forms a hollow ring 160 Å in diameter and 85 Å high (Fig. 3). The central lumen has an average diameter of ~35 Å, narrowing to ~20 Å in some places; it is polar and negatively charged (Fig. 3d),

consistent with the cation selectivity of PA_{63} channels, but also includes a conserved phenylalanine (Phe 427) in a solvent-exposed loop. Monomers pack like pie wedges, with domains 1′ and 2 on the inside of the ring and domains 3 and 4 on the outside. Heptamer formation entails no major conformational changes in the monomers, and buries an extensive surface (2,200 $Å^2$ per monomer) composed primarily of charged or polar residues from domain 2 and domain 1′. The buried surface is fully accessible in the monomeric PA structure, but substituting full-length PA for PA_{63} in the heptamer results in a severe overlap among the seven PA_{20} moieties, showing that heptamerization before furin cleavage is sterically blocked. Residues in the interface are highly conserved, suggesting that the homologous toxins also oligomerize.

The tertiary structure of domain 1′ remains largely unchanged on heptamer formation, despite rupture of the β-sheet. The largest movement occurs in the $1\beta_{12}$–$1\beta_{13}$ hairpin, which tilts upwards (by 5 Å at its tip) to avoid steric clashes with its neighbour. The domain is stabilized by an extensive interface with domain 2 and internally by the two calcium ions, which link the new N terminus to residues in the core of domain 1′ and prevent its becoming disordered. The new hydrophobic surface on domain 1′ is completely exposed, forming part of a large, flat, hydrophobic patch on the 'top' of the heptamer (Fig. 3c). This surface provides an obvious site for binding oedema factor and lethal factor, which bind PA_{63} with high affinity[2,16] but cannot bind full-length PA. Monoclonal antibody studies also implicate domain 1′ (and the adjacent domain 3) in oedema/lethal factor binding[10].

Because lethal factor binds cells preincubated with PA_{63} and blocks the ion conductance of preformed PA_{63} membrane channels[16], the membrane-bound heptamer is likely to be oriented with domain 1′ exposed to the extracellular environment, available to bind oedema factor and lethal factor, and with domain 4 and the bottom of domain 2 next to the membrane. How does the heptamer insert into membranes? Our heptamer structure lacks an obvious belt of hydrophobic residues, but proteolysis and mutagenesis experiments have implicated the large $2\beta_2$–$2\beta_3$ loop of domain 2 (residues 302–325, a chymotrypsin-sensitive loop with two Phe residues at its tip) in the intoxication process[11,17]. Electrophysiological measurements on the membrane-inserted heptamer involving point mutations in this loop place residues 304, 306 and 308 inside the channel lumen (E. L. Benson, P. D. Huynh, A. Finkelstein and R.J.C., unpublished data). The loop shows a conserved pattern of alternating hydrophilic and hydrophobic residues, similar to that seen in porins (Fig. 4a) and in the membrane-spanning hairpin of α-haemolysin from *Staphylococcus aureus*[18]. In α-haemolysin, each monomer contributes an amphipathic hairpin to a 14-stranded β-

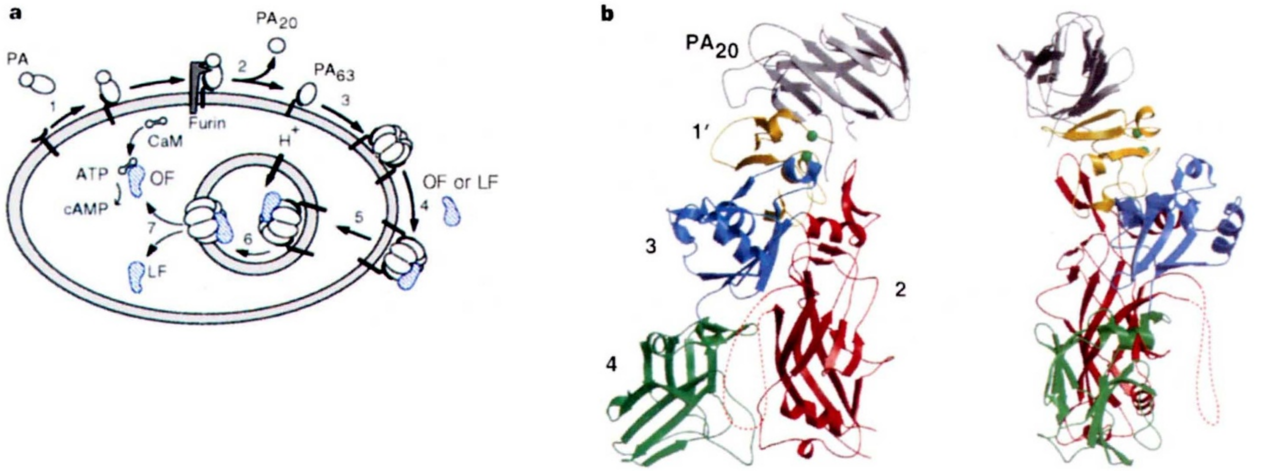

c

1β1 1β2 1β3 1β4 1β5
EVKQENRLLNESESSSQGLLGYYFSDLNFQAPMVVTSSTTGDLSIPSSELENIPSENQYFQSAIWSGFIKVKKSDEYTFA 80

1β6 1β7 1β8 1β9 1β10 1β11
TSADNHVTMWVDDQEVINKASNSNKIRLEKGRLYQIKIQYQRENPTEKGLDFKLYWTDSQNKKEVISSDNLQLPELKQKS 160

Furin 1α1 1β12 1β13 1α2 1β14 1α3
SNSRKKRSTSAGPTVPDRDNDGIPDSLEVEGYTVDVKNKRTFLSPWISNIHEKKGLTKYKSSPEKWSTASDPYSDFEKVT 240

1α4 2β1 2β2 Chymotrypsin
GRIDKNVSPEARHPLVAAYPIVHVDMENIILSKNEDQSTQNTDSETRTISKNTSTSRTHTSEVHGNAEVHASFFDIGGSV 320

2β3 2α1 2β4 2β5 2β6 2β7
SAGFSNSNSSTVAIDHSLSLAGERTWAETMGLNTADTARLNANIRYVNTGTAPIYNVLPTTSLVLGKNQTLATIKAKENQ 400

2β8 2β9 2β10 2β11 2α2 2β12 2β13 2β14
LSQILAPNNYYPSKNLAPIALNAQDDFSSTPITMNYNQFLELEKTKQLRLDTDQVYGNIATYNFENGRVRVDTGSNWSEV 480

2α3 3β1 3β2 3α1 3β3 3α2 3β4 3β5 3β6
LPQIQETTARIIFNGKDLNLVERRIAAVNPSDPLETTKPDMTLKEALKIAFGFNEPNGNLQYQGKDITEFDFNFDQQTSQ 560

3α3 3α4 3β7 3β8 4β1 4β2 4α1 4β3 4β4 4α2
NIKNQLAELNATNIYTVLDKIKLNAKMNILIRDKRFHYDRNNIAVGADESVVKEAHREVINSSTEGLLLNIDKDIRKILS 640

4β5 4β6 4β7 4β8 4β9
GYIVEIEDTEGLKEVINDRYDMLNISSLRQDGKTFIDFKKYNDKLPLYISNPNYKVNVYAVTKENTIINPSENGDTSTNG 720

4β10 4α3
IKKILIFSKKGYEIG

Figure 1 a, Steps in anthrax intoxication. 1, PA binds to a host cell receptor; 2, furin cleaves and releases PA_{20}; 3, PA_{63} forms a heptamer; 4, the toxic enzymes bind to PA_{63}; 5, receptor-mediated endocytosis; 6, acidification of the endosome leads to membrane insertion of PA_{63}; 7, translocation of the toxic enzymes into the cytosol. LF, lethal factor; EF, oedema factor. **b**, Orthogonal views of PA, coloured by domain. Domain 1 comprises PA_{20} (grey) plus domain 1′ (yellow), and two Ca^{2+} ions (green spheres). **c**, Secondary structure assignment. Highly conserved (underlined), moderately conserved (marked by a dot) and invariant (bold) residues are indicated, as are residues ligating calcium ions through side-chain (circled) or main-chain atoms (boxed).

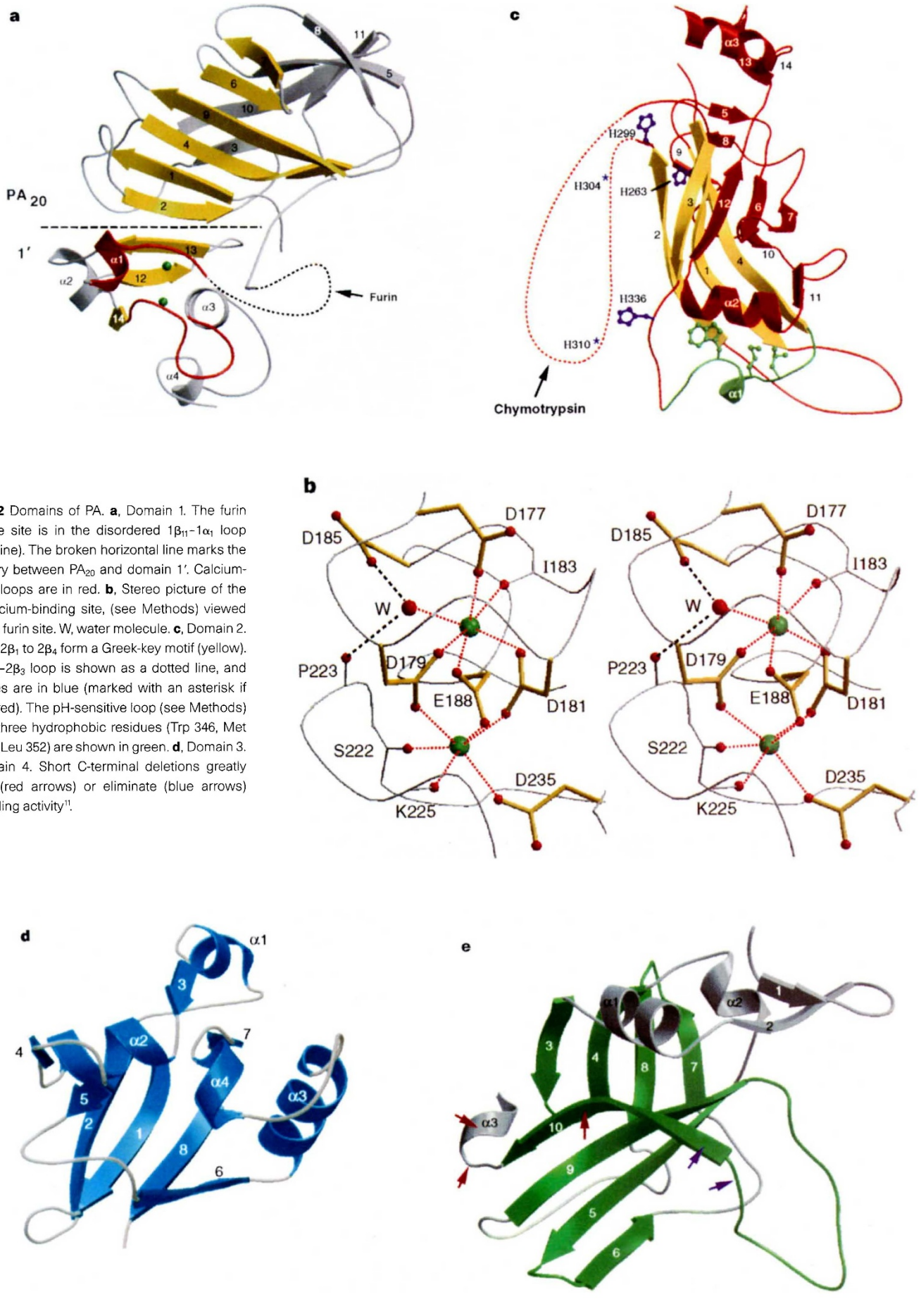

Figure 2 Domains of PA. **a**, Domain 1. The furin cleavage site is in the disordered $1\beta_{11}$-$1\alpha_1$ loop (dotted line). The broken horizontal line marks the boundary between PA_{20} and domain 1′. Calcium-binding loops are in red. **b**, Stereo picture of the twin calcium-binding site, (see Methods) viewed from the furin site. W, water molecule. **c**, Domain 2. Strands $2\beta_1$ to $2\beta_4$ form a Greek-key motif (yellow). The $2\beta_2$-$2\beta_3$ loop is shown as a dotted line, and histidines are in blue (marked with an asterisk if disordered). The pH-sensitive loop (see Methods) and its three hydrophobic residues (Trp 346, Met 350 and Leu 352) are shown in green. **d**, Domain 3. **e**, Domain 4. Short C-terminal deletions greatly reduce (red arrows) or eliminate (blue arrows) cell-binding activity[11].

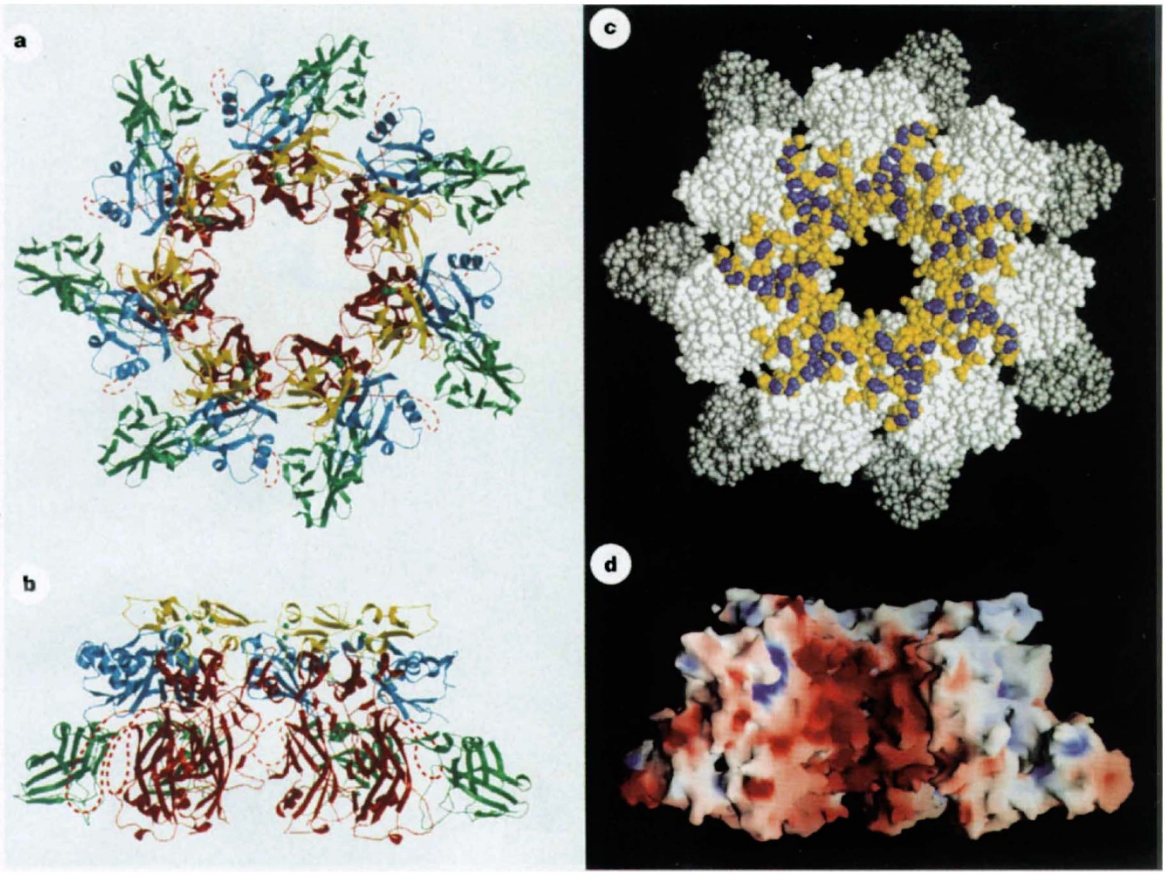

Figure 3 The PA_{63} heptamer. **a**, Axial view, coloured as in Fig. 1b. **b**, Side view, with three monomers removed to reveal the heptamer interior. **c**, Space-filling model, viewed as in **a**. PA_{20} removal exposes a large surface area (~1,600 Å^2 per monomer, yellow and blue), of which 40% is due to hydrophobic side chains (blue). **d**, The heptamer lumen, viewed as in **b**. Regions of positive (blue) and negative (red) surface potential are indicated. Generated with GRASP[29]. Homology models of VIP1 and iota-*b* also have a negatively charged lumen, suggesting that this feature may be important for translocation, an acid-dependent process[2]. The lumen is too small to allow the passage of native folded lethal (or oedema) factor, but large enough to accommodate helices and sub-domains.

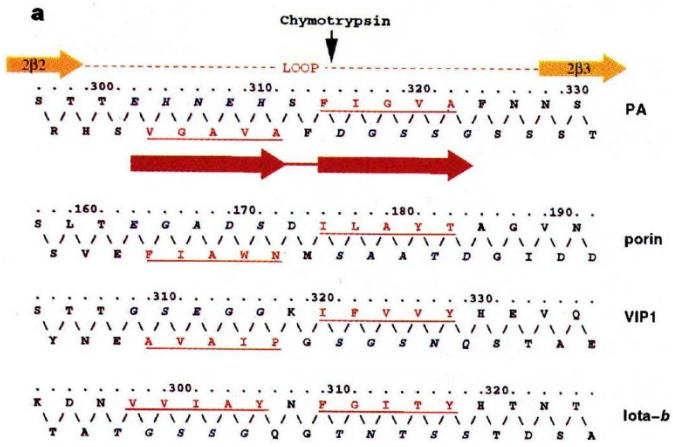

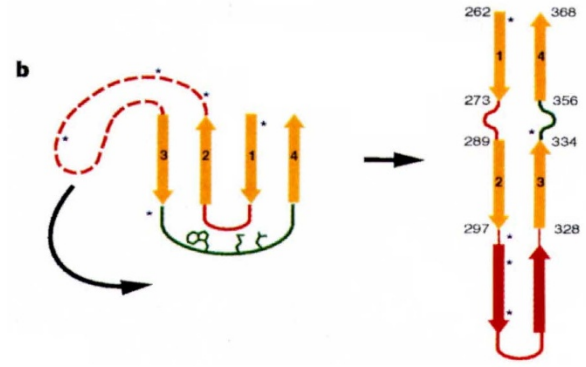

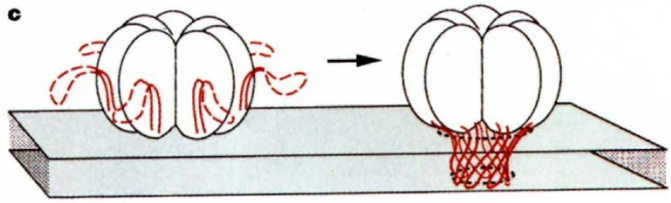

Figure 4 Model of membrane insertion. **a**, Amphipathic hairpin formation by the $2\beta_2$-$2\beta_3$ loop of PA and its homologues, with residues forming the hydrophobic face in red and the hydrophilic face in blue. A membrane-spanning hairpin from *Rhodopseudomonas blastica* porin[30] is shown for comparison. Cleavage at the chymotrypsin site eliminates toxicity. **b**, Unfolding of the Greek-key motif (strands $2\beta_1$ to $2\beta_4$) to form a β-hairpin extending from the base of domain 2 to the heptamer axis. Histidine positions are shown as blue asterisks. Residues that undergo the order-to-disorder transition in crystals of PA are shown in green. **c**, Association of the seven β-hairpins in the PA_{63} heptamer to form a 14-stranded, membrane-inserted β-barrel.

Table 1 Crystallographic statistics

Monomeric PA

Data set	Nat1a	Nat1b	Nat2	MMN1*	MMN2	MA	K_2PtCl_4	K_2PtBr_6	TTP	U	KI
Resolution (Å)	3.2	2.5	2.1	3.2	3.2	4.0	3.6	3.2	3.6	4.0	3.4
Unique	13,012	28,421	45,183	11,423	13,129	6,686	9,359	12,073	8,180	7,112	10,093
Completeness (%)	90	96	91	85	90	92	96	83	82	94	89
Redundancy	7.0	3.3	3.0	4.2	3.8	2.9	2.4	2.6	3.3	4.0	4.3
R_{sym} (%)†	4.1	6.6	6.7	4.7	9.9	4.5	4.0	7.0	5.1	7.0	7.1
$\langle I\rangle/\langle\sigma I\rangle$ in outer shell	4.8	10.7	4.0	3.4	1.5	8.2	6.6	4.8	4.2	3.8	3.5
Sites				5	6	5	2	3	2	4	11
R_{iso}*				8.9	22.3	13.0	11.3	13.9	12.5	11.0	13.1
R_{Cullis}‡				0.72	0.71	0.86	0.90	0.80	0.81	0.89	0.88
Phasing power				1.1	1.2	0.7	0.6	0.9	0.6	0.5	0.6
Mean overall figure of merit (20-3.2 Å)				0.58							

Refinement statistics:	Resolution (Å)	*R* factor (%)§	R_{free} (%)‖	R.m.s. bond lengths (Å)¶	R.m.s. bond angles (deg)¶
crystal form 1	6-2.5	27.1	32.0	0.009	2.0°
crystal form 2	6-2.1	22.3	29.1	0.006	1.5°

Heptameric PA_{63}

Resolution shell (Å)	9.63	7.64	6.67	6.06	5.63	5.30	5.03	4.81	4.63	4.47	Overall
Unique	3,876	3,924	3,894	3,899	3,856	3,882	3,897	3,894	3,869	2,969	37,959
Completeness (%)	96.5	99.2	99.4	99.4	99.5	99.4	99.7	99.6	99.6	76.6	99.1
Redundancy	2.7	2.8	2.8	2.8	2.8	2.8	2.8	2.8	2.8	2.1	2.8
$\langle I\rangle/\langle\sigma I\rangle$	20.6	16.2	9.9	7.4	5.8	5.1	4.4	4.2	3.9	2.6	9.8
R_{sym} (%)†	3.3	5.0	10.2	14.6	18.9	22.9	26.3	27.7	29.7	32.1	10.2
Statistics of non-crystallographic symmetry phase refinement:											
Averaging *R*#	19.0	17.7	20.4	24.0	26.6	29.6	31.1	33.5	38.0	49.9	23.9
Correlation☆	0.91	0.91	0.90	0.85	0.83	0.78	0.74	0.71	0.67	0.55	0.87

* Abbreviations for heavy-metal derivatives are defined in the Methods section.
† $Rsym = \Sigma\Sigma_i |\langle I\rangle - I_i| / \Sigma\langle I\rangle$. † $R_{iso} = \Sigma |F_{ph} - F_p| / F_p|$.
‡ $R_{Cullis} = \Sigma ||F_{ph} \pm F_p| - F_{ph}| / \Sigma |F_{ph} \pm F_p|$ for centric reflections.
§ *R* factor $= \Sigma ||F_p| - |F_{p\,calc}|| / \Sigma F_p$ for reflections with $F_p > 2\sigma(F_p)$.
‖ R_{free} is computed on a randomly selected 10% of the data which were excluded from refinement.
¶ The r.m.s. deviations from ideal values.
# Averaging $R = \Sigma |F_O - F_C| / \Sigma |F_O|$.
☆ Correlation coefficient $= \Sigma_h(\langle F_O\rangle - |F_{Oh}|)(\langle F_C\rangle - |F_{Ch}|) / \{\Sigma_h(\langle F_O\rangle - |F_{Oh}|)^2 - (\langle F_C\rangle - |F_{Ch}|)^2\}^{1/2}$.

barrel, and we propose that PA inserts into membranes in an analogous fashion. The diameter of PA_{63} membrane channels determined by solute exclusion (~12 Å)[19] is consistent with the size of such a barrel.

The $2\beta_2$–$2\beta_3$ loops project outwards from the side of the water-soluble heptamer (Fig. 3). Their assembly into a β-barrel on the heptamer axis could be accomplished most simply if the Greek-key motif formed by the first four strands of domain 2 ($2\beta_1$ to $2\beta_4$) were to unfold, with strands $2\beta_2$ and $2\beta_3$ peeling away from the edge of the domain (Figs 4 and 2c). This would involve breaking about as many hydrogen bonds as are created on barrel formation, and is analogous to the conformational change proposed for the pH-induced conversion of transthyretin from its native to its amyloidogenic form[20]. *In vivo*, the trigger for membrane insertion is provided by acidification of the endosome. *In vitro*, channel formation by PA_{63} in planar lipid bilayers is accelerated rapidly when the pH is lowered from 7.4 to 6.5 (refs 15, 21), implicating the titration of histidines. Of the nine histidines in PA_{63}, five are contained within the Greek-key motif of domain 2 (Fig. 2c and 4b). Two histidines (His 304 and His 310) lie within the $2\beta_2$–$2\beta_3$ loop. Two others (His 263 and His 299) form part of an unusual cluster of buried polar residues (including three arginines (Arg 297, Arg 490 and Arg 504) and one glutamate (Glu 502)) located at the top of the Greek key where the $2\beta_2$–$2\beta_3$ loop joins the body of domain 2. Local instability induced by protonation of these histidines would be relieved if strands $2\beta_2$ and $2\beta_3$ peeled away to expose the charged residues to solvent. The fifth histidine (His 336) lies at the bottom of the Greek key in the loop connecting strands $2\beta_3$ and $2\beta_4$. Residues in this loop are ordered in crystals of PA grown at pH 7.5, but are disordered in the crystal form grown at pH 6.0, exposing three hydrophobic residues to solvent. This order-to-disorder transition may resemble the initial conformational changes that occur in the heptamer during membrane insertion. □

Methods

Structure determination of monomeric PA. (See Table 1.) Crystal form 1 grows in 14–18% PEG 1000, 10% glycerol and 50 mM HEPES, pH 7.5, at 4 °C, and adopts space group $P2_12_12_1$ with $a = 119.8$ Å, $b = 73.8$ Å, $c = 95.0$ Å. Crystal form 2 grows in 12–18% PEG 18K and 50 mM citrate, pH 6.0, at 4 °C, and belongs to space group $P2_12_12_1$ with $a = 99.3$ Å, $b = 93.7$ Å, $c = 82.0$ Å. All data sets listed in Table 1 except Nat2 are from crystal form 1. Three native data sets were used: Nat1a for the multiple isomorphous replacement (MIR) phasing, and Nat1b and Nat2 for refinement. Nat1b was collected at 4 °C at SSRL beamline 7-1 ($\lambda = 1.08$ Å) on a MAR image plate, while Nat2 was collected at −170 °C using 30% PEG 200 as the cryoprotectant on a CCD area detector at CHESS beamline A-1 ($\lambda = 0.92$ Å). Nat1b and Nat2 were processed with DENZO and SCALEPACK[22]. All other data sets were collected at 4 °C on a Xuong-Hamlin Multiwire area detector using Cu Kα radiation, and were processed with UCSD software[23]. Crystal form 1 was solved by MIR. Soaking conditions for heavy-metal derivatives were as follows: MMN1 and MMN2, methylmercuric nitrate at 1 mM for 5 h and 10 mM for 1 h, respectively; MA, 10 weeks in 10 mM mersalyl acid; K_2PtCl_4, 3 days at 10 mM; K_2PtBr_6, 3 days at 2 mM and 3 days at 4 mM; TTP, 2 days in 5 mM dipotassium tetrakis(thiocyanato)platinate (II); $UO_2(NO_3)_2$, 0.1–1 mM over 4 days; KI_3, 6 days in 10 mM KI_3. Heavy-atom positions were determined by Patterson and cross-Fourier methods, and atomic parameters were refined using MLPHARE[24]. An MIR map calculated at 3.5 Å showed a clear solvent boundary and several elements of secondary structure. An initial model consisting of ~300 glycine and alanine residues was built using FRODO[25] and refined at 2.5 Å resolution with XPLOR[26]. Recombining model phases with the experimental phases led to an improved map and allowed additional residues to be modelled. The initial sequence assignment was facilitated by iodinating crystals to specifically label

tyrosines and by mercurating crystals of two point mutants, Thr → Cys at 357 and Ser → Cys at 623. Iterative cycles of phase recombination, manual model building and XPLOR refinement led to a nearly complete model, but several ambiguities persisted. These were resolved using crystal form 2, whose structure was solved by molecular replacement and refined at 2.1 Å resolution. Two strong peaks of density in an $F_o - F_c$ map were identified as calcium ions on the basis of coordination geometry, bond distances, and the prevalence of acidic ligands. The presence of calcium was confirmed by atomic absorption spectroscopy (T. Koehler and R.J.C., unpublished data). The two calcium ions are 4.3 Å apart and are bridged by three carboxylate groups. Ca1 (top calcium ion in Fig. 2b) is in a calcium-binding loop like that in the canonical EF-hand[27], coordinated by carboxylate oxygens of Asp 177, Asp 179, Asp 181 and Glu 188, the carbonyl oxygen of Ile 183, and a water molecule. Ca2 (lower calcium ion in Fig. 2b) is in a novel motif, coordinated by carboxylate oxygens of Asp 179, Asp 181, Glu 188 and Asp 235, and the carbonyl oxygens of Ser 222 and Lys 225. The model for crystal form 2 consists of 660 (of 735) residues, 390 water molecules, and 2 calcium ions. The model for crystal form 1 contains 680 residues, 2 calcium ions and no water molecules, and will be further refined. No density is seen in either crystal form for residues 1–13, 162–176 and 304–319, consistent with the protease sensitivity of these regions[14]. Residues 343–350 shown in green in Figs 2c and 4b, including the three hydrophobic residues indicated (Trp 346, Met 350 and Leu 352), are ordered in crystal form 1 (pH 7.5) and in the PA_{63} heptamer (pH 8.5), but are disordered in crystal form 2 (pH 6.0). Residues 511–516 of domain 3 form helix $3\alpha_1$ in crystal form 1 and in the PA_{63} heptamer, but are disordered in crystal form 2.

Structure determination of heptameric PA_{63}. (See Table 1.) Crystals grow at room temperature in 2–5% PEG 8K, 10 mM $CaCl_2$ and 50 mM Tris, pH 8.5, and belong to space group $P2_12_1$, with $a = 142.8$ Å, $b = 148.3$ Å, $c = 164.1$ Å and $\beta = 107.9°$. Data were collected at −170 °C using 30% ethylene glycol as a cryoprotectant on a MAR image plate at the ESRF beamline BM14 ($\lambda = 0.945$ Å). A self-rotation function revealed a peak on the $\kappa = 51°$ section that was 68% as high as the origin peak, indicating the presence of one heptamer per asymmetric unit, with the 7-fold axis parallel to the crystallographic 2-fold screw along *b*. A cross-rotation function calculated using domains 1′ to 4 of the monomer structure gave an unambiguous solution at 8.5 σ above the mean, and other strong peaks related by non-crystallographic symmetry. A translation search for one monomer gave a clear peak at 9.9 σ above the mean, with the highest noise peak at 2.9 σ. Clear solutions were also obtained for the other monomers which, when placed relative to the same origin by a combined translation function, gave a centre of mass in good agreement with the position deduced from the native Patterson. The heptamer model showed good packing in the crystal, and was consistent with electron micrographs. Rigid body refinement of the 7 monomers caused a drop in the crystallographic *R*-factor from 0.48 to 0.41, and a similar drop in R_{free} (calculated using thin shells of reflections comprising 5% of unique measurements). An additional drop in R_{free} was obtained by refining the four domains of each monomer as independent rigid bodies. The resulting coordinates were used to define the non-crystallographic symmetry operators. Cycles of 7-fold averaging were performed with RAVE[28], starting from a set of random phases and a mask derived from the atomic coordinates. The averaging *R*-factor converged to 23.9% for all measurements from 40 to 4.5 Å, and the real-space correlation coefficients relating the monomers were all 0.90 or higher. The rigid-body refined model showed good fit to the averaged map, which showed well-resolved backbone density but little density for side chains. The strongest features in the map were at 6 σ above the mean, and corresponded to the calcium ion sites. Minor conformational changes were readily apparent, including shifts in individual helices in domains 1′ and 3 and a shift in the hairpin formed by residues 194–204. The model was adjusted in these regions, and further rigid-body refinement led to a crystallographic *R*-factor of 32% and an R_{free} of 36%. The model has not been further refined, owing to a lack of high-resolution data.

Received 6 September 1996; accepted 3 January 1997.

1. Turnbull, P. in *Topley and Wilson's Principles of Bacteriology, Virology and Immunity: Bacterial Diseases* (eds Smith, G. R. & Easman, C. S. F.) 365–379 (Arnold, London, 1990).
2. Leppla, S. H. in *Bacterial Toxins and Virulence Factors in Disease* (eds Moss, J., Iglewksi, B., Vaughan, M. & Tu, A. T.) 543–572 (Dekker, New York, 1995).
3. Milne, J. C. & Collier, R. J. pH-dependent permeabilization of the plasma membrane of mammalian cells by anthrax protective antigen. *Mol. Microbiol.* **10,** 647–653 (1993).
4. Milne, J. C., Furlong, D., Hanna, P. C., Wall, J. S. & Collier, R. J. Anthrax protective antigen forms oligomers during intoxication of mammalian cells. *J. Biol. Chem.* **269,** 20607–20612 (1994).
5. Blanke, S. R., Milne, J. C., Benson, E. L. & Collier, R. J. Fused polycationic peptide mediates delivery of diphtheria toxin A chain to the cytosol in the presence of antrhrax protective antigen. *Proc. Natl Acad. Sci. USA* **93,** 8437–8442 (1996).
6. Arora, N. & Leppla, S. H. Residues 1–254 of anthrax toxin lethal factor are sufficient to cause cellular uptake of fushed polypeptides. *J. Biol. Chem.* **268,** 3334–3341 (1993).
7. Prasad, G. S. *et al.* Structure of toxic shock syndrome toxin-1. *Biochemistry* **32,** 13761–13766 (1993).
8. Perelle, S., Gibert, M., Boquet, P. & Popoff, M. R. Characterization of *Clostridium perfringens* Iota-Toxin genes and expression in *Escherichia coli*. *Infect. Immun.* **61,** 5147–5156 (1993).
9. Warren, G. *et al. Novel pesticidal proteins and strains.* World intellectual property organization. Patent application WO 96/10083 (1996).
10. Little, S. F. *et al.* Characterization of lethal factor-binding and cell-receptor binding domains of protective antigen of *Bacillus anthracis* using monoclonal antibodies. *Microbiology* **142,** 707–715 (1996).
11. Novak, J. M., Stein, M.-P., Little, S. F., Leppla, S. H. & Friedlander, A. M. Functional characterization of protease-treated *Bacillus anthracis* protective antigen. *J. Biol. Chem.* **267,** 17186–17193 (1992).
12. Singh, Y., Klimpel, K. R., Quinn, C. P., Chaudhary, V. K. & Leppla, S. H. The carboxyl-terminal end of protective antigen is required for receptor binding and anthrax toxin activity. *J. Biol. Chem.* **266,** 15493–15497 (1991).
13. Choe, S. *et al.* The crystal structure of diphtheria toxin. *Nature* **357,** 216–222 (1992).
14. Leppla, S. H. in *Sourcebook of Bacterial Protein Toxins* (eds Alouf, J. E. & Freer, J. H.) 277–302 (Academic, San Diego, 1991).
15. Blaustein, R. O., Koehler, T. M., Collier, R. J. & Finkelstein, A. Anthrax toxin: channel-forming activity of protective antigen in planar phospholipid bilayers. *Proc. Natl Acad. Sci. USA* **86,** 2209–2213 (1989).
16. Zhao, J., Milne, J. C. & Collier, R. J. Effect of anthrax toxin's lethal factor on ion channels formed by the protective antigen. *J. Biol. Chem.* **270,** 18626–18630 (1995).
17. Singh, Y., Klimpel, K. R., Arora, N., Sharma, M. & Leppla, S. H. The chymotrypsin-sensitive site, FFD^{315}, in anthrax toxin protective antigen is required for translocation of lethal factor. *J. Biol. Chem.* **269,** 29039–29046 (1994).
18. Song, L. *et al.* Structure of Staphylococcal α-hemolysin, a heptameric transmembrane pore. *Science* **274,** 1859–1865 (1996).
19. Blaustein, R. O. & Finkelstein, A. Voltage-dependent block of anthrax toxin channels in planar phospholipid bilayer membranes by symmetric tetraalkylammonium ions. *J. Gen. Physiol.* **96,** 905–919 (1990).
20. Kelly, J. W. Alternative conformations of amyloidogenic proteins govern their behavior. *Curr. Opin. Struct. Biol.* **6,** 11–17 (1996).
21. Koehler, T. M. & Collier, R. J. Anthrax toxin protective antigen: low pH-induced hydrophobicity and channel formation in liposomes. *Mol. Microbiol.* **5,** 1501–1506 (1991).
22. Otwinowski, Z. in *Data collection and processing* (eds Sawyer, L., Isaacs, N. & Bailey, S.) 56–62 (SERC Daresbury Laboratory, Warrington, UK, 1993).
23. Howard, A. J. *et al.* Software for a diffractometer with multiwire area detector. *Methods Enzymol.* **114,** 452–472 (1985).
24. Otwinowski, Z. in *Proceedings of the CCP4 Study Weekend: Isomorphous Replacement and Anomalous Scattering* 80–85 (SERC Daresbury Laboratory, Warrington, UK, 1991).
25. Jones, T. A. A graphics model building and refinement system for macromolecules. *J. Appl. Crystallogr.* **11,** 268–272 (1978).
26. Brünger, A. T. *X-PLOR Manual, version 3.1* (Yale University, New Haven, CT, 1992).
27. Nakayama, S. & Kretsinger, R. H. Evolution of the EF-Hand family of proteins. *Annu. Rev. Biophys. Biomol. Struct.* **23,** 473–507 (1994).
28. Kleywegt, G. & Jones, T. A. in *From First Map to Final Model* (eds Bailey, S., Hubbard, R. & Waller, D.) 59–66 (SERC Daresbury Laboratory, Warrington, UK, 1994).
29. Nicholls, A. *GRASP: Graphical Representation and Analysis of Surface Properties* (Columbia University, New York, 1992).
30. Kreusch, A., Neubüser, A., Schiltz, E., Weckesser, J. & Schultz, G. E. The structure of the membrane channel porin from *Rhodopseudomonas blastica* at 2.0 Å resolution. *Protein Sci.* **3,** 58–63 (1994).

Acknowledgements. We thank the staff at CHESS, SSRL and the ESRF for use of their facilities, and are grateful to G. Leonard for technical assistance. We also thank J.-O. Lee, K. Taraszka and H. Y. Liu for early contributions to the work on PA; J. Milne for electron micrographs of the heptamer; T. Koehler for atomic absorption spectroscopy results; P. Hanna, E. L. Benson, G. Warren and H. Bayley for discussions; and L. Bankston and J. Cabral for critical reading of the manuscript. Much of this work was carried out while C.P. and R.C.L. were at Harvard Medical School and the Dana-Farber Cancer Institute, and was supported by the US Army Medical Research Institute of Infectious Diseases.

Correspondence and requests for materials should be addressed to C.P. (e-mail: cppl@leicester.ac.uk).
Coordinates have been deposited with the Protein Data Bank (1acc).